

Effect of Spray Distance on Microstructure and Tribological Performance of Suspension Plasma-Sprayed Hydroxyapatite–Titania Composite Coatings

Chao Zhang, Haifeng Xu, Xin Geng, Jingjing Wang, Jinkun Xiao, and Peizhi Zhu

(Submitted May 27, 2016; in revised form July 25, 2016)

Hydroxyapatite (HA)--titania (TiO₂) composite coatings prepared on Ti6Al4V alloy surface can combine the excellent mechanical property of the alloy substrate and the good biocompatibility of the coating material. In this paper, HA–TiO₂ composite coatings were deposited on Ti6Al4V substrates using suspension plasma spray (SPS). X-ray diffraction, scanning electron microscopy, Fourier infrared absorption spectrometry and friction tests were used to analyze the microstructure and tribological properties of the obtained coatings. The results showed that the spray distance had an important influence on coating microstructure and tribological performance. The amount of decomposition phases decreased as the spray distance increased. The increase in spray distance from 80 to 110 mm improved the crystalline HA content and decreased the wear performance of the SPS coatings. In addition, the spray distance had a big effect on the coating morphology due to different substrate temperature resulting from different spray distance. Furthermore, a significant presence of OH⁻ and CO₃²⁻ was observed, which was favorable for the biomedical applications.

Keywords hydroxyapatite-titania coatings, microstructure, suspension plasma spray, tribological performance

1. Introduction

Hydroxyapatite (HA) has a good biocompatibility with skin, muscle and other soft tissues, as well as with bone and other hard tissues (Ref 1-5). After implantation in the human body, HA exhibits no side effects and is favorable to induce the growth of bones (Ref 6-8). Therefore, HA is considered to be the most appropriate hard tissue replacement materials in the medical field (Ref 9). However, as a ceramic material, HA gives poor mechanical properties, such as low plasticity, low bending strength and weak impact resistance, which results in an inability to bear a large force.

This article is an invited paper selected from presentations at the 2016 International Thermal Spray Conference, held May 10–12, 2016, in Shanghai, P. R. China, and has been expanded from the original presentation.

Chao Zhang, Haifeng Xu, Xin Geng, Jingjing Wang, and Jinkun Xiao, College of Mechanical Engineering, Yangzhou University, Yangzhou 25127, People's Republic of China; and Xin Geng and Peizhi Zhu, College of Chemistry and Chemical Engineering, Yangzhou University, Yangzhou 225002, People's Republic of China. Contact e-mails: zhangc@yzu.edu.cn and zhangchao_cqu@hotmail.com.

The materials for artificial joint implant require high strength, good wear resistance and suitable elastic modulus close to the human bone (Ref 2). At present, the typical method is to deposit HA coatings on the titanium alloy substrates, like Ti6Al4V, in order to plot the good mechanical properties of the alloy and the good biocompatibility from hydroxyapatite. In artificial hip, the hydroxyapatite is often coated on femoral stems and on the outer surface of acetabula cups. The mechanisms that may lead to the detachment of the HA coating may be mechanical or biochemical, or a mixture. Mechanical mechanism involves abrasion, insertion, fatigue and micro-motion. Biochemical mechanism includes dissolution into body fluid, cell-mediated processes and crystallization. The detachment of coating is affected by many factors such as coating method, the raw powder morphology, processing parameters, coating thickness and coating structure (Ref 10). HA particles might be liberated from the coating due to the movement at the implant–bone interface. Therefore, wear becomes a problem in the long-term service period as it may result in a poor mechanical fit between the ball and socket of the hip which can lead to loosening of the prostheses and this can ultimately lead to failure of the artificial implant (Ref 11). In order to prolong the service life of the artificial implant, the wear resistance of HA coating should be taken into account.

The incorporation of TiO₂ into HA improved the corrosion rate (Ref 12), bonding strength and biocompatibility (Ref 13). The in vitro studies (Ref 13) showed that the HA particles in HA–TiO₂ coating are bigger in size and Ca/P ratio was higher than pure HA. In addition,

compared with the single HA coating, the HA–TiO₂ composite coating benefited dental implants in both primary (mechanical) and secondary (bio-inductive) stability stages (Ref 14). HA–TiO₂ coatings were intensively studied by many researchers with various processes, like electrophoretic deposition (Ref 12), sol–gel (Ref 14) and plasma electrolytic oxidation (Ref 14, 15).

The conventional process for the deposition of HA coating is atmospheric plasma spray (APS) (Ref 16). APS is an ultra-high temperature and rapid process. The dehydration and decomposition of HA phase cannot be avoided, and the decomposition phases, like dehydroxylated oxyapatite, alpha and beta tricalcium phosphate and tetra calcium phosphate and amorphous calcium phosphate, may be produced during the APS process. This problem is fatal since either of them is instable in body fluid and results in unexpected coating failure ahead of service time. Therefore, it is important to optimize the spray parameters to get at least 50% of pure crystalline HA (ISO13779-2) within the obtained coating. Suspension plasma spray has a great potential to achieve high-crystallinity HA coatings because that the decomposition phases may react with water molecules to reform stable HA (Ref 17). The reformation of HA has been confirmed in a conventional APS HA coating subjected to a post-steam treatment (Ref 18). Moreover, nanostructured HA coatings have been successfully prepared by suspension plasma spray (SPS) process (Ref 19). SPS could also be envisaged favorably to produce HA–TiO₂ coatings. Although HA–TiO₂ were prepared by different thermal spray processes, such as flame spray (Ref 20), high velocity oxygen fuel (Ref 21), APS (Ref 22, 23) and SPS (Ref 24–27), there are few reports focusing on the tribological performance of HA–TiO₂ coatings.

In the present article, HA–TiO₂ composite coatings were deposited on Ti6Al4V substrates using SPS process. Various analytical techniques have been used to characterize the coating microstructure. Then, reciprocating sliding tests of the coatings were carried out under dry and simulated body fluid (SBF)-lubricated conditions. The effects of spray distance on coating microstructure, phase

structure, chemical composition and tribological properties were studied.

2. Experimental Methods

2.1 Liquid Feedstock

The HA suspension was prepared by a wet chemical method. 0.24 mol/L (NH₄)₂HPO₄ aqueous solution was added into stirred 0.4 mol/L Ca(NO₃)₂ aqueous solution according to a Ca/P atomic ratio of 1.67. The pH value of the solution was adjusted to 10 with ammonia (NH₄OH) solution. The reaction was kept at 95 °C for four days. Subsequently, the solution was aged for two days and then dialyzed with deionized water to remove ammonia. Then, 40 g/L hydroxyapatite suspension was obtained. Commercial TiO₂ suspension was purchased from Hangzhou WanJing New Material Co., Ltd. The concentration was 200 g/L. 0.035 L TiO₂ suspension was added into 1 L HA suspension to get a composite suspension with mass ratio of 15:85 wt.% (TiO₂:HA). The particle sizes and morphologies of the HA precursor, TiO₂ nanoparticles and composite were observed by transmission electron microscopy (TEM, Tecnai 12, Philips, Netherlands), as shown in Fig. 1(a–c), respectively.

2.2 Coating Deposition

HA–TiO₂ coatings were prepared on Ti6Al4V substrates by suspension plasma spray with a F4MBXL plasma spray gun (Oerlikon Metco, Switzerland). A six-axis ABB robot (ABB, Sweden) was used to move the spray torch in order to get a uniform and reproducible deposition. Prior to spraying, the substrates were grit-blasted with 24 mesh corundum. The suspension was driven through a peristaltic pump and injected into the plasma flame by a nozzle with an inner diameter of 0.26 mm. The flow rate of the suspension was controlled at 35 mL/min. The primary plasma gas was argon with a flow rate of 50 L/min, and the secondary plasma gas was hydrogen with a flow rate of 4 mL/min. In order to study

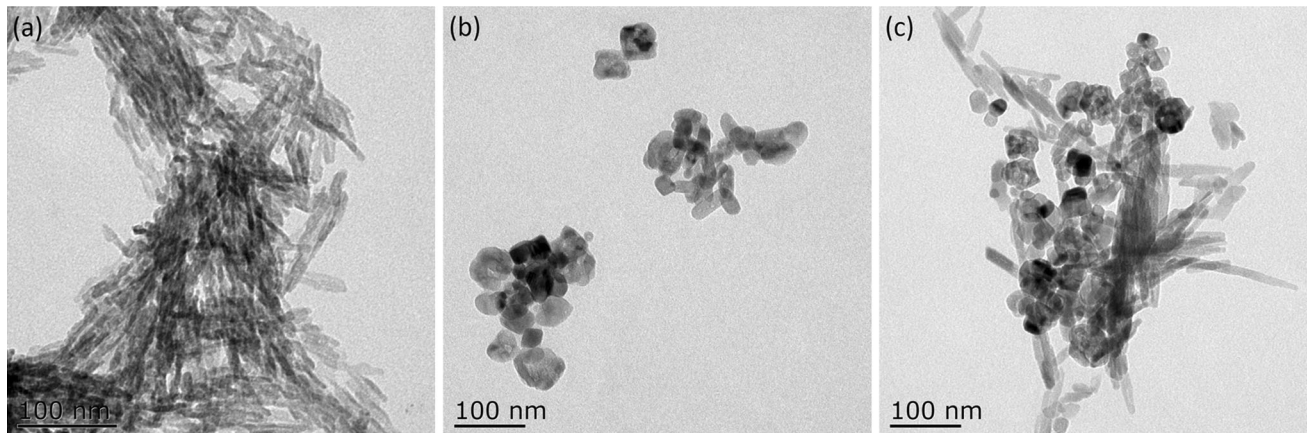


Fig. 1 TEM images of (a) HA nanowires, (b) TiO₂ nanospheres and (c) HA–TiO₂ composite

the influence of spray distance on coating properties, the spray distances of 80, 90, 100 and 110 mm were adopted, respectively. Dry compressed air, supplied at 2.5 bar, was used as cooling gas for the substrates. SPS parameters were listed in Table 1.

2.3 Coating Characterization

The coating surface was inspected by field emission scanning electron microscopy (FE-SEM, S4800 II, Hitachi, Japan). X-ray diffraction (XRD, D8ADVANCE, BRUKER/AKS, Germany) analysis of the specimens was performed on an x-ray diffractometer (CuK α radiation) with 2 θ diffraction angle ranging from 20° to 60°. Fourier transform infrared spectroscopy (FTIR, Cary 610/670, Varian, USA) were performed on the obtained coatings. For FTIR, the coatings were firstly removed from the substrate and then grinded into powder. The spectra were recorded from 4000 to 450 cm $^{-1}$.

2.4 Friction and Wear Tests

The friction and wear tests were carried out in linear reciprocating ball-on-disk configuration using a tribometer (UMT-2, Bruker, USA), with stainless ball of ϕ 4 mm as counterpart. The samples were tested with a fixed sliding speed of 10 mm/s, a reciprocating stroke of 8 mm and a normal load of 0.2 N. The wear tracks were measured by

Table 1 SPS spray parameters

Parameters	Value
Arc current (A)	513
Spray distance (mm)	80, 90, 100 and 110
Ar (L/min)	50
H $_2$ (L/min)	4
Liquid Nozzle (mm)	0.26
Suspension feed rate (mL/min)	35
Torch scan speed (mm/min)	300
Pass spacing (mm)	3

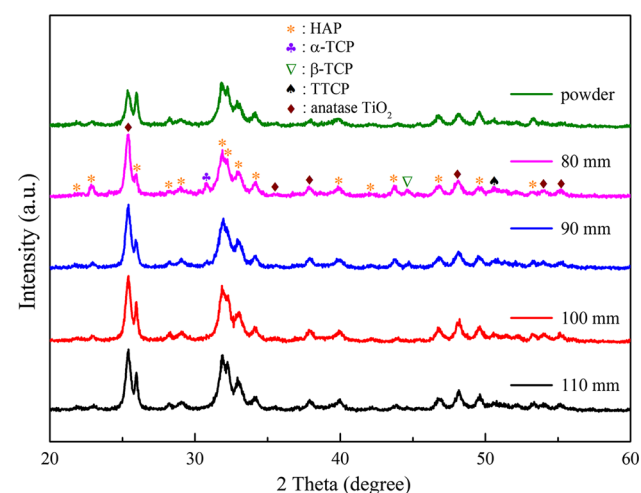


Fig. 2 X-ray diffraction patterns of the four HA-TiO $_2$ coatings

3D optical profilometer (GT-K, Bruker, USA), and the volume loss for each specimens was calculated using Vision64 $^{\text{®}}$ imaging topography software.

3. Results and Discussion

3.1 Phase Structure

Figure 2 shows the XRD patterns of the liquid feedstock and HA-TiO $_2$ coatings deposited at spray distances of 80, 90, 100 and 110 mm. The as-synthesized suspension was firstly freeze-dried into powder and then characterized by XRD, and the result demonstrated that only HA and TiO $_2$ phases existed in the liquid feedstock. It can be observed that the main peaks of the four coatings belong to HA and anatase TiO $_2$. When the spray distance was reduced from 100 to 90 and 80 mm, α -tricalcium phosphate (α -TCP), β -tricalcium phosphate (β -TCP), tetracalcium phosphate (TTCP) appear. HA nanowires were melted in the high-temperature plasma flame during SPS processing. As a result, HA was dehydroxylated and decomposed. Generally speaking, dehydroxylation and decomposition of HA are associated. At 800-900 °C, partial dehydroxylation leads to form oxygen-vacant hydroxyapatite (Ca $_{10}$ (PO $_4$) $_6$ (OH) $_{0.5}$ O $_{0.75}$). When the temperature is further increased to above 1050 °C, oxygen-vacant hydroxyapatite was decomposed into β -TCP, α -TCP and TTCP. Further to observe in Fig. 2, the β -TCP, α -TCP and TTCP peaks belonging to the coatings deposited by 110 mm were the smallest, while those with spray distance of 80 mm were the biggest. It means that the amount of decomposition phases in the as-sprayed coatings decreases as the spray distance increases. The SPS provided less energy for HA compared with APS due to partial energy consumption by water, which results in less HA decomposition. In addition, the decomposition phases can react with water molecules and reform again the HA phase (Ref 19). When the spray distance was reduced to 90 and 80 mm, the plasma flame almost touched

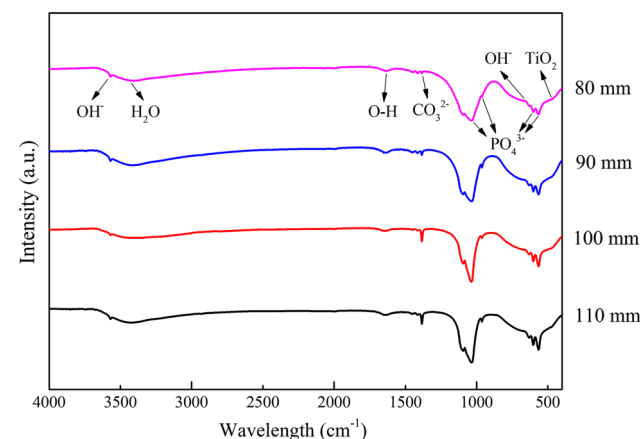


Fig. 3 FT-IR spectra of the four HA-TiO $_2$ coatings

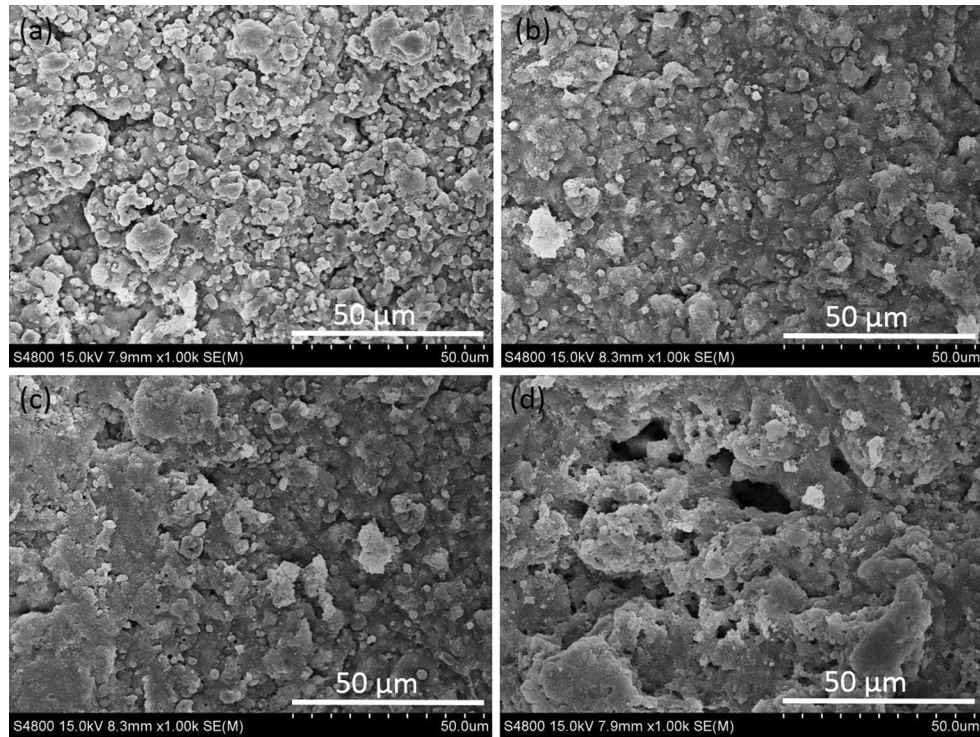


Fig. 4 Low-magnification surface morphology of the coatings deposited at (a) 80 mm, (b) 90 mm, (c) 100 mm and (d) 110 mm

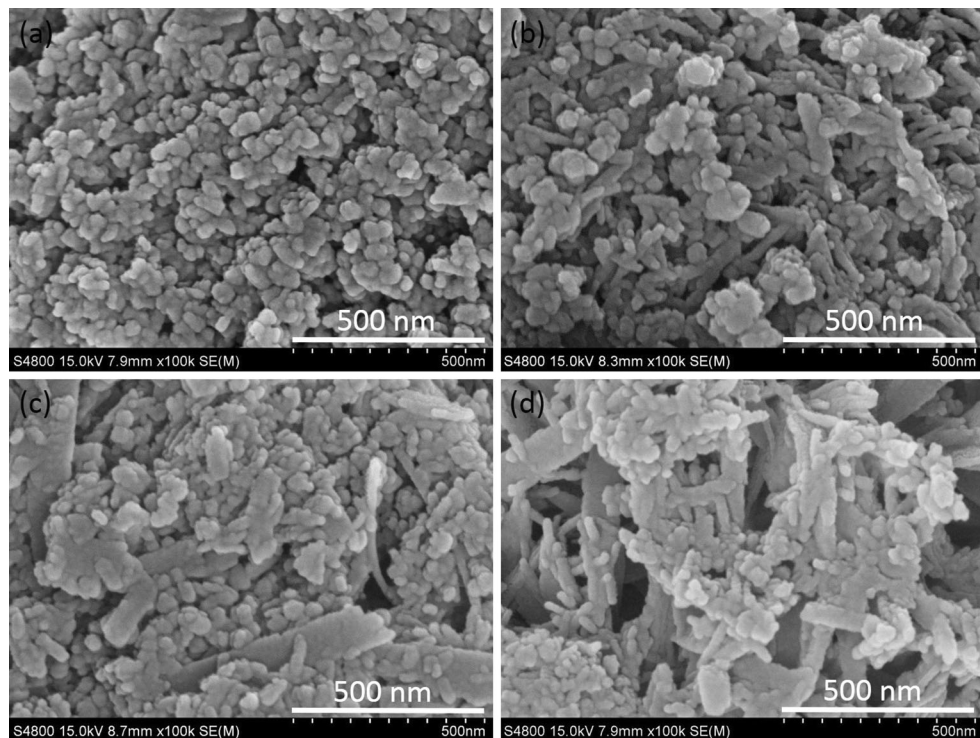


Fig. 5 High-magnification surface morphology of the coatings deposited at (a) 80 mm, (b) 90 mm, (c) 100 mm and (d) 110 mm

the substrate and gave an actual annealing on the deposited particle leading to partial decomposition of HA coatings. Even so, it can be observed that all the main HA

peaks are retained in the 80 and 90 mm coatings. It can be pointed out that SPS process can obviously alleviate the decomposition of the HA powders.

In addition, the content of hydroxyapatite is notoriously related to the biological and bioactive performance of the as-sprayed coatings. Therefore, it is imperative to estimate the hydroxyapatite phase's content. In this study, the external standard and Diffrac Eva software were used to calculate the hydroxyapatite content, which was also reported in (Ref 28). The hydroxyapatite content is 55.7, 63.4, 68.3 and 72.9% when the spray distance is 80, 90, 100 and 110, respectively. It can be concluded that the content of hydroxyapatite increases with the spray distance and the coating deposited at 110 mm distance has the highest content. As it is well known, the plasma plume is about 70 mm long. When the spray distance of 80 mm is utilized, the temperature of the substrate is so high leading to the decomposition of hydroxyapatite. As the spray distance increases, the temperature of substrate decrease and less hydroxyapatite would decompose, which increases the hydroxyapatite content in the as-sprayed coatings.

FTIR spectra of the four HA-TiO₂ coatings deposited at 80, 90, 100 and 110 mm are given in Fig. 3. The main absorption peaks can be ascribed to OH⁻, H₂O, O-H, CO₃²⁻ and PO₄³⁻, as labeled in the figure. The CO₃²⁻ can be produced by adsorbed CO₂ and OH⁻ in the alkaline HA suspension (Ref 19). The 560-570 cm⁻¹ feature is the asymmetric stretching vibration peak of PO₄³⁻. The 950-960 cm⁻¹ peak is related to the symmetric stretching vibration peak of PO₄³⁻, while that at 1000-1200 cm⁻¹ is associated with asymmetric bending vibration peaks of PO₄³⁻. Features at 630 and 3570 cm⁻¹ are the absorption peaks of OH⁻, while that at 3300-3500 cm⁻¹ is the absorption peak of H₂O. The obvious OH⁻ peak can be observed in the spectrum, which means that most of the

stoichiometric hydroxyapatite was retained even if particles flow through the ultra-high-temperature plasma plume. In atmospheric plasma-sprayed hydroxyapatite coatings, the most intense problem is dehydroxylation due to the high temperature provided by the plasma flame, so the obtained coatings generally need to be post-treated to recover the OH⁻ groups. However, the problem of dehydroxylation is alleviated in the SPS hydroxyapatite coatings, which simplifies the fabrication process. Moreover, it also can be found that the peak intensities for CO₃²⁻ groups increase when a long spray distance is used.

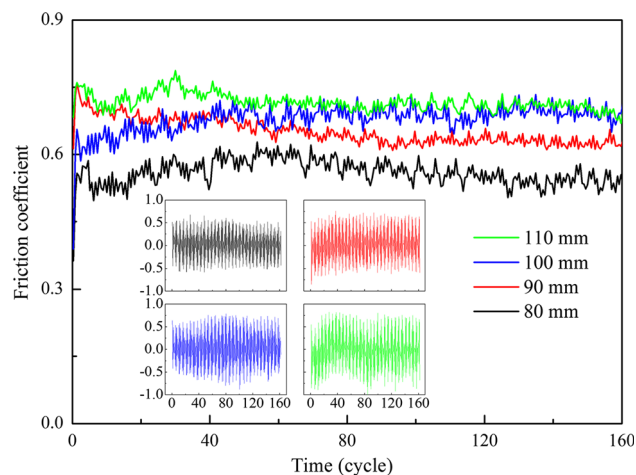


Fig. 7 Average friction coefficient curves of the four coatings under dry conditions, inset: raw friction coefficient curves

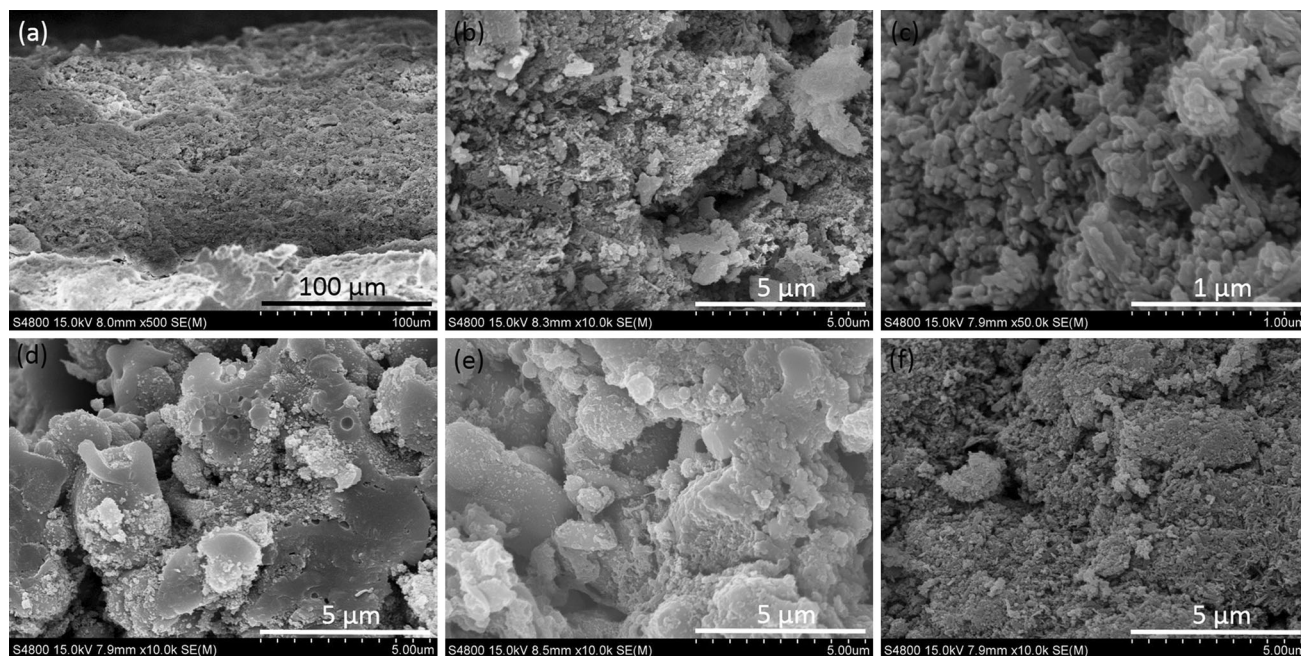


Fig. 6 FE-SEM images of fractured cross-sectional surface morphology of the 100 mm coating at a magnification of (a) 500 \times , (b) 10,000 \times and (c) 50,000 \times ; 80 mm coating at a magnification (d) 10,000 \times ; 90 mm coating at a magnification (e) 10,000 \times ; 110 mm coating at a magnification (f) 10,000 \times

The presence of CO_3^{2-} can effectively enhance the combination between the as-sprayed coatings and the bone as well as the tissue in the simulated body fluid (Ref 19). As it is well known, the CO_3^{2-} is easily decomposed to CO_2 at high temperature. So when a short spray distance is utilized, less CO_3^{2-} will be retained in the coatings.

3.2 Coating Microstructure

Figure 4 shows the surface morphology of SPS HA-TiO₂ coatings under 1000× magnification. HA and TiO₂ particles are melted or partially melted at high temperature and impact on the substrate surface. Due to the short spray distance, the front end of the plasma plume was

close to the substrate surface, which gave a heat on the deposited particles and led to the partially decomposition of the hydroxyapatite during spraying. When the spray distance increased from 80 to 90, 100 and 110 mm, the agglomerated particles are gradually reduced on the coating surface. When the spray distance is 110 mm, almost no agglomerated particles can be observed. Meanwhile, more pores exist in the coatings, especially when the spray distance reaches 100 and 110 mm. It can be measured that the size of pores in the 110 mm coating is above 10 μm. In order to observe the coating nanostructure, the four coatings were inspected under 100,000× magnification, as shown in Fig. 5. When the spray distance is 80 mm, the powders were well melted, and HA nanowires were melted into nanospheres with a size of 30-50 nm. When the spray distance increased to 90, 100 and 110 mm, HA nanowires began to be retained in the coatings. The length of HA wires was about 200-250 nm, and the widths were ranging from 30 to 70 nm. When the spray distance is short than the length of plasma flame, the plasma flame directly heats the substrate and the pre-deposited particles. As a result, the HA wires were melted into nanospheres. The coatings with Ti6Al4V substrates were cut by a metallographic cutting machine, and the cross-sectional surface was observed by SEM. Figure 6 shows the cross-sectional surface morphology of the coating deposited at 100 mm. It can be estimated that the HA-TiO₂ coatings have a thickness of 100 μm.

It was pointed out that higher porosity and pore size had a positive effect on bone ingrowth and would result in enhanced osteoconductive properties, which was favorable for the mechanical bonding between bone tissue and implant (Ref 29). In view of the unique pore architecture in plasma sprayed coatings, the surface makes a good biological binding between coating and human tissues, which will be beneficial to the growth of human tissue.

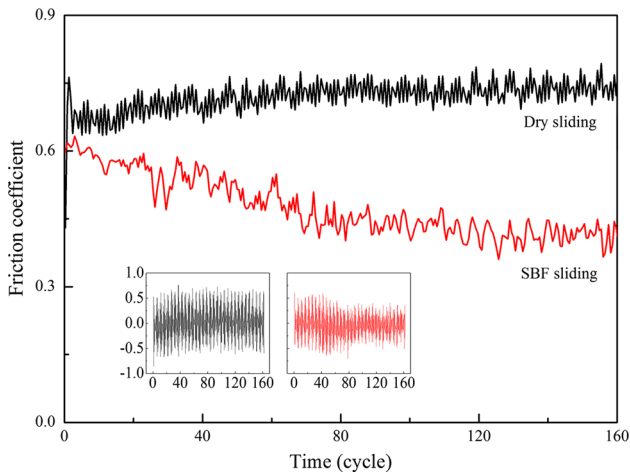


Fig. 8 Average friction coefficient curves of the 80 mm coating under dry and SBF-lubricated conditions, inset: raw friction coefficient curves

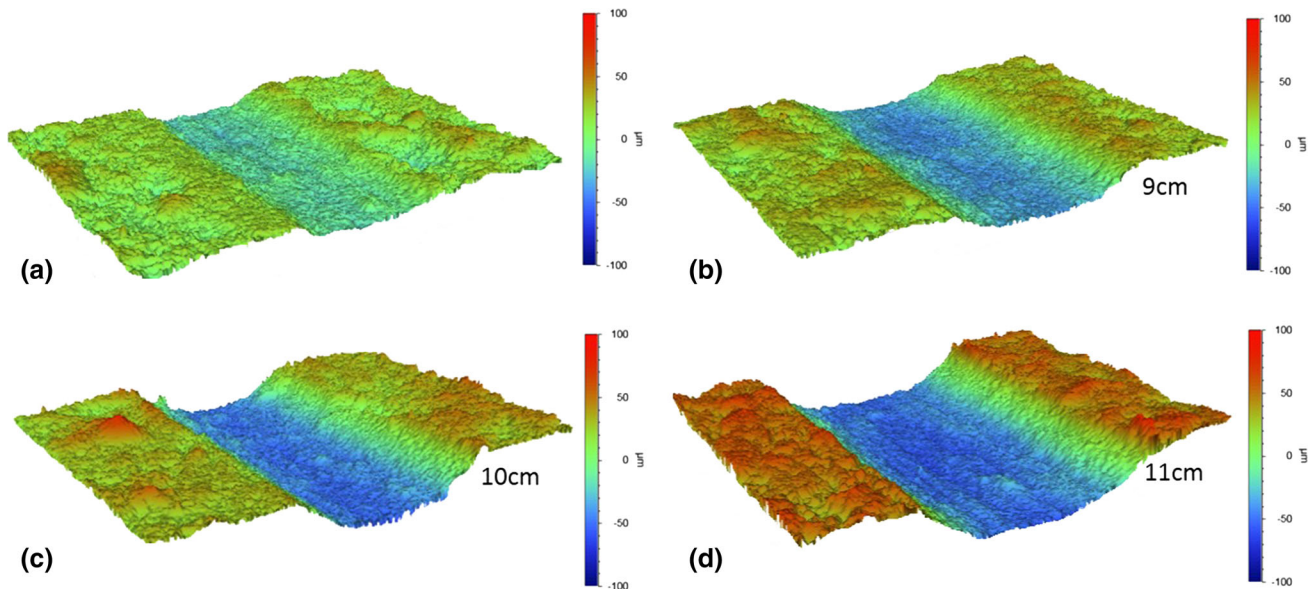
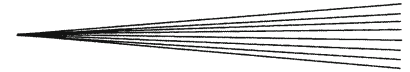


Fig. 9 3D images on the wear tracks of the coatings deposited at (a) 80 mm, (b) 90 mm, (c) 100 mm and (d) 110 mm



3.3 Tribological Performance

Figure 7 shows the average friction coefficients of the coatings deposited at 80, 90, 100 and 110 mm under dry sliding condition. It can be found that the friction coefficients of the coatings were almost stable during sliding. With the increase in spray distance, the coating becomes more porous. At first, the rough surface makes the sliding contact only occur in the convex part. The friction coefficient quickly increases to stable values in the first two cycles. The friction coefficient of the coating prepared at

80 mm is significantly lower than those of the coatings deposited at longer distances, which should be attributed to the coating microstructure as shown in Fig. 6. It can be concluded that the friction performance was improved when the spray distance decreased from 110 to 80 mm. Figure 8 presents the average friction coefficient of the 80 mm coating under dry condition and simulated body fluid (SBF)-lubricated conditions. Under SBF-lubricated condition, the friction coefficient firstly decreased gradually and then became stable. The coefficient was significantly lower than that under dry condition. Therefore, it

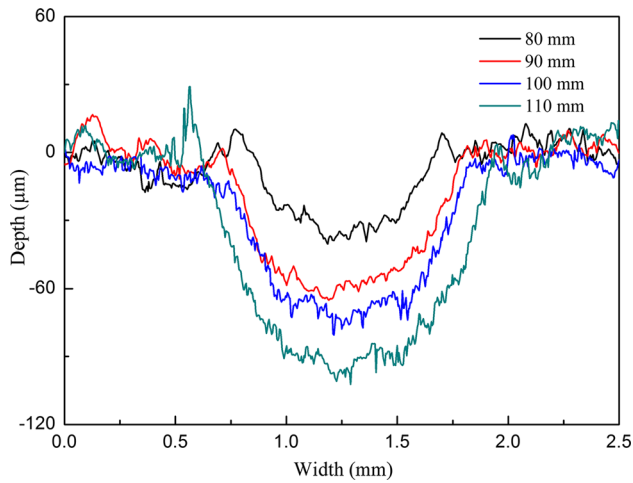


Fig. 10 Cross-sectional profiles of wear tracks of the four coatings after dry sliding

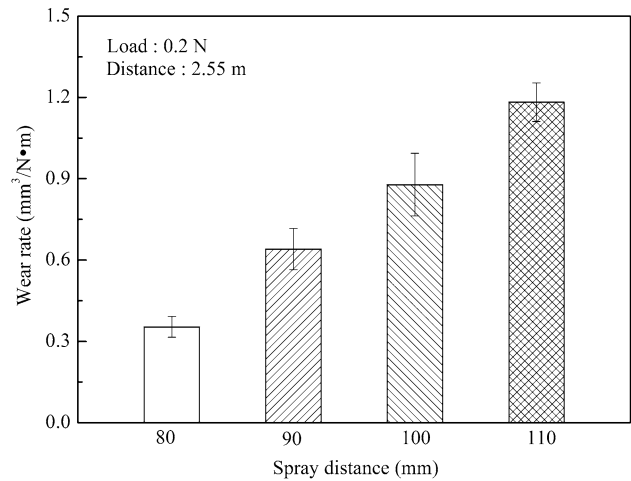


Fig. 12 Wear rate of the four coatings under dry sliding

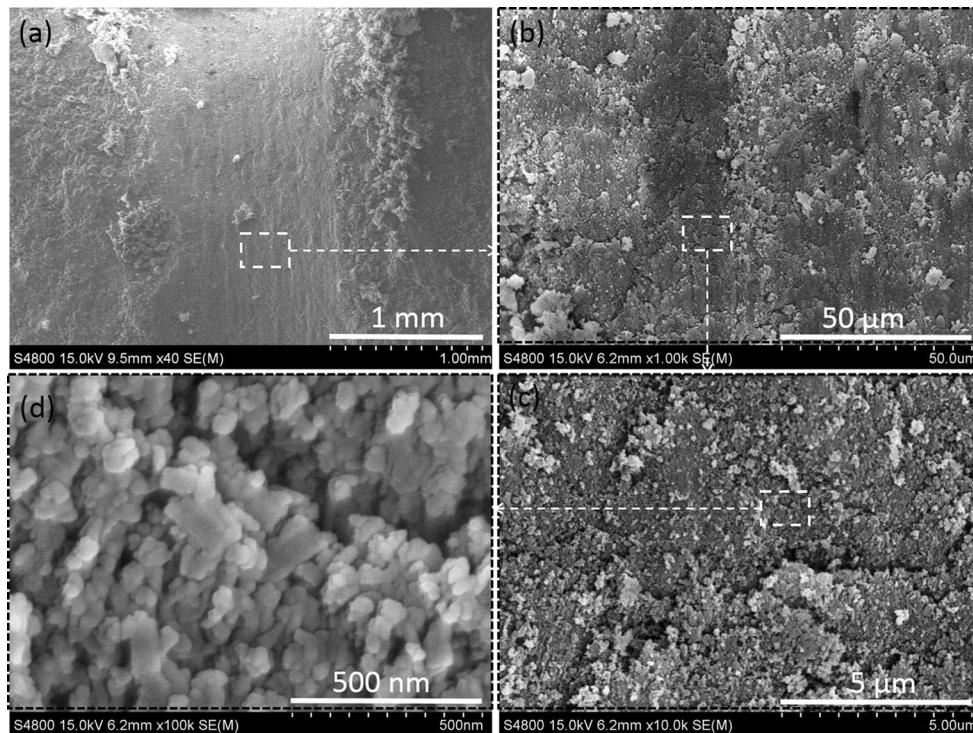


Fig. 11 FE-SEM images of worn surface morphology of the sliding track of the 100 mm coating after the dry sliding at a magnification of (a) 40 \times , (b) 1000 \times , (c) 10,000 \times and (d) 100,000 \times

can be seen that the SBF played a role in lubricating, which effectively reduced the friction coefficient.

3D images on the tracks of the four specimens after dry sliding are taken, as shown in Fig. 9. It can be seen that the track depth increases with spray distance. The cross-sectional profile of the tracks are extracted and listed in Fig. 10. After 160 cycles, the track depth reaches to 35, 60, 72 and 95 μm for the four coatings. The depth increased almost linearly with the increase in spray distance, which is in accordance with the tendency of friction coefficient. The worn surfaces of the coatings after sliding were inspected by SEM. All the coatings showed similar sliding behavior, as shown in Fig. 11. The worn debris were distributed on the two sides and two ends of the sliding track. The wear mechanism which was involved in this study should be abrasive wear, since the particle cohesion was limited. The wear rate of the specimens was calculated and depicted in Fig. 12. It increased from 0.35 ± 0.04 , 0.64 ± 0.08 , 0.88 ± 0.12 and $1.18 \pm 0.07 \text{ mm}^3/\text{N}\cdot\text{m}$ when the spray distance increased from 80 to 90, 100 and 110 mm. It should be mentioned that the depth of the track was about 100 μm when the spray distance increased to 110 mm. The depth reached almost the thickness of the coating, which means the friction may be influenced by the Ti6Al4V substrate, especially when the sliding approached to the substrate.

4. Conclusions

In this paper, HA–TiO₂ composite coatings were successfully deposited on Ti6Al4V substrate by suspension plasma spray. XRD results showed that there was no obvious decomposition of HA in the coatings deposited at 110 and 100 mm, while a small part of HA was decomposed to TCP and TTCP in the coatings deposited at 90 and 80 mm. The HA nanowires were transformed to nanospheres when the spray distance was 80 mm. When the spray distance was increased to 90, 100 and 110 mm, HA wires were retained in the coatings, and they became short and thick compared with the nanowires in the suspension feedstock. The sliding tests were performed under dry and SBF-lubricated conditions. The friction coefficient and wear rate decreased when the spray distance decreased from 110 to 80 mm. Increasing the spray distance improved the HA phase content whereas the tribological performance was worsened. Therefore, a compromise should be made in order to obtain a balance between the HA phase content and tribological performance.

Acknowledgments

This work was supported by the Natural Science Foundation of China (51402255), the Jiangsu Natural Science Foundation of China (BK20140487) and the Testing Center of Yangzhou University. This work was also supported by Cooperation Fund of Yangzhou City—Yangzhou University (YZ2016254) and a project funded by the Priority Academic Program Development of Jiangsu higher education institutions.

References

1. Z.S. Stojanović, N. Ignjatović, V. Wu, V. Žunić, L. Veselinović, S. Skapin, M. Miljković, V. Uskoković, and D. Uskoković, Hydrothermally Processed 1D Hydroxyapatite: Mechanism of Formation and Biocompatibility Studies, *Mater. Sci. Eng., C*, 2016, **68**, p 746-757
2. S. Zhang, *Hydroxyapatite Coatings for Biomedical Applications*, CRC Press, Boca Raton, 2013
3. L. Sun, C.C. Berndt, and C.P. Grey, Phase, Structural and Microstructural Investigations of Plasma Sprayed Hydroxyapatite Coatings, *Mater. Sci. Eng., A*, 2003, **360**, p 70-84
4. B. Ben-Nissan, A. Milev, and R. Vago, Morphology of Sol-Gel Derived Nano-Coated Coralline Hydroxyapatite, *Biomaterials*, 2004, **25**, p 4971-4975
5. S. Vahabzadeh, M. Roy, A. Bandyopadhyay, and S. Bose, Phase Stability and Biological Property Evaluation of Plasma Sprayed Hydroxyapatite Coatings for Orthopedic and Dental Applications, *Acta Biomater.*, 2015, **17**, p 47-55
6. H. Huang, P. Lan, Y. Zhang, X. Li, X. Zhang, C. Yuan, X. Zheng, and Z. Guo, Surface Characterization and In Vivo Performance of Plasma-Sprayed Hydroxyapatite-Coated Porous Ti6Al4V Implants Generated by Electron Beam Melting, *Surf. Coat. Technol.*, 2015, **283**, p 80-88
7. B.C. Wang, E. Chang, C.Y. Yang, D. Tu, and C.H. Tsai, Characteristics and Osteoconductivity of Three Different Plasma-Sprayed Hydroxyapatite Coatings, *Surf. Coat. Technol.*, 1993, **58**, p 107-117
8. M. Monsalve, H. Ageorges, E. Lopez, F. Vargas, and F. Bolivar, Bioactivity and Mechanical Properties of Plasma-Sprayed Coatings of Bioglass Powders, *Surf. Coat. Technol.*, 2013, **220**, p 60-66
9. R.I.M. Asri, W.S.W. Harun, M.A. Hassan, S.A.C. Ghani, and Z. Buyong, A Review of Hydroxyapatite-Based Coating Techniques: Sol-Gel and Electrochemical Depositions on Biocompatible Metals, *J. Mech. Behav. Biomed. Mater.*, 2016, **57**, p 95-108
10. C. Dunne, J. Gibbons, D. FitzPatrick, K. Mulhall, and K. Stanton, On the Fate of Particles Liberated from Hydroxyapatite Coatings in Vivo, *Ir. J. Med. Sci.*, 2015, **184**, p 125-133
11. B. Ratner, A. Hoffman, F. Schoen, and J.E. Lemons, *Biomaterial Science: An Introduction to Materials in Medicine*, Elsevier, Amsterdam, 2004
12. H. Farnoush, J.A. Mohandesib, and H. Çimenogluç, Micro-Scratch and Corrosion Behavior of Functionally Graded HA–TiO₂ Nanostructured Composite Coatings Fabricated by Electrochemical Deposition, *J. Mech. Behav. Biomed. Mater.*, 2015, **46**, p 31-40
13. P. Amaravathy, S. Sathyanarayanan, S. Sowndarya, and N. Rajendran, Bioactive HA/TiO₂ Coating on Magnesium Alloy for Biomedical Applications, *Ceram. Int.*, 2014, **40**, p 6617-6630
14. T. Cheng, Y. Chen, and X. Nie, Insertion Torques Influenced by Bone Density and Surface Roughness of HA–TiO₂ Coatings, *Thin Solid Films*, 2013, **549**, p 123-130
15. D. Dzhurinskiy, Y. Gao, W.-K. Yeung, E. Strumban, V. Leshchinsky, P.-J. Chu, A. Matthews, A. Yerokhin, and R. Gr Maev, Characterization and Corrosion Evaluation of TiO₂: n-HA Coatings on Titanium Alloy Formed by Plasma Electrolytic Oxidation, *Surf. Coat. Technol.*, 2015, **269**, p 258-265
16. K. De Groot, R. Geesink, C.P.A.T. Klein, and P. Serekian, Plasma Sprayed Coatings of Hydroxylapatite, *J. Biomed. Mater. Res.*, 1987, **21**, p 1375-1387
17. W. Tong, J. Chen, Y. Cao, L. Lu, J. Feng, and X. Zhang, Effects of Water Vapor Pressure and Temperature on the Amorphous-to-Crystalline HA Conversion During Heat Treatment of HA Coatings, *J. Biomed. Mater. Res.*, 1997, **36**, p 242-245
18. Y. Cao, J. Weng, and J. Chen, Water Vapour-Treated Hydroxyapatite Coatings After Plasma Spraying and their Characteristics, *Biomaterials*, 1996, **17**, p 419-424
19. H. Xu, X. Geng, G. Liu, J. Xiao, D. Li, Y. Zhang, P. Zhu, and C. Zhang, Deposition, Nanostructure and Phase Composition of Suspension Plasma-Sprayed Hydroxyapatite Coatings, *Ceram. Int.*, 2016, **42**, p 8684-8690



20. Y. Liu, J. Huang, S. Ding, Y. Liu, J. Yuan, and H. Li, Deposition, Characterization, and Enhanced Adherence of Escherichia Coli Bacteria on Flame-Sprayed Photocatalytic Titania-Hydroxyapatite Coatings, *J. Therm. Spray Technol.*, 2013, **22**, p 1053-1062
21. S. Dimitrievska, M.N. Bureau, J. Antoniou, F. Mwale, A. Petit, R.S. Lima, and B.R. Marple, Titania-Hydroxyapatite Nanocomposite Coatings Support Human Mesenchymal Stem Cells Osteogenic Differentiation, *J. Biomed. Mater. Res.*, 2011, **98**, p 576-588
22. X.B. Zheng and C.X. Ding, Characterization of Plasma-Sprayed Hydroxyapatite/TiO₂ Composite Coatings, *J. Therm. Spray Technol.*, 2000, **9**, p 520-525
23. F.X. Ye, A. Ohmori, T. Tsumura, K. Nakata, and C.J. Li, Microstructural Analysis and Photocatalytic Activity of Plasma-Sprayed Titania-Hydroxyapatite Coatings, *J. Therm. Spray Technol.*, 2007, **16**, p 776-782
24. R. Jaworski, L. Pawlowski, C. Pierlot, F. Roudet, S. Kozerski, and F. Petit, Recent Developments in Suspension Plasma Sprayed Titanium Oxide and Hydroxyapatite Coatings, *J. Therm. Spray Technol.*, 2010, **19**, p 240-247
25. G. Bolelli, D. Bellucci, V. Cannillo, L. Lusvardi, A. Sola, N. Stiegler, P. Müller, A. Killinger, R. Gadow, L. Altomare, and L. De Nardo, Suspension Thermal Spraying of Hydroxyapatite: Microstructure and In Vitro Behavior, *Mater. Sci. Eng.*, 2014, **34**, p 287-303
26. B. Pateyron, L. Pawlowski, N. Calve, G. Delluc, and A. Denoirjean, Modeling of Phenomena Occurring in Plasma Jet During Suspension Spraying of Hydroxyapatite Coatings, *Surf. Coat. Technol.*, 2013, **214**, p 86-90
27. S. Kozerski, L. Pawlowski, R. Jaworski, F. Roudet, and F. Petit, Two Zones Microstructure of Suspension Plasma Sprayed Hydroxyapatite Coatings, *Surf. Coat. Technol.*, 2010, **204**, p 1380-1387
28. T. Candidato, P. Sokolowski, L. Pawlowski, and A. Denoirjean, Preliminary Study of Hydroxyapatite Coatings Synthesis Using Solution Precursor Plasma Spraying, *Surf. Coat. Technol.*, 2015, **277**, p 242-250
29. V. Karageorgiou and D. Kaplan, Porosity of 3D Biomaterial Scaffolds and Osteogenesis, *Biomaterials*, 2005, **26**, p 5474-5491